The Astrophysical Journal, 764:152 (10pp), 2013 February 20 doi:10.1088/0004-637X/764/2/152

THE CONTRIBUTION OF RADIO GALAXY CONTAMINATION TO MEASUREMENTS OF THE SUNYAEV–ZEL'DOVICH DECREMENT IN MASSIVE GALAXY CLUSTERS AT 140 GHz WITH BOLOCAM

J. Sayers[1], T. Mroczkowski[1,2,7], N. G. Czakon[1], S. R. Golwala[1], A. Mantz[3], S. Ameglio[4], T. P. Downes[1], P. M. Koch[5], K.-Y. Lin[5], S. M. Molnar[6], L. Moustakas[2], S. J. C. Muchovej[1], E. Pierpaoli[4], J. A. Shitanishi[4], S. Siegel[1], and K. Umetsu[5]

[1] Division of Physics, Math, and Astronomy, California Institute of Technology, Pasadena, CA 91125, USA; jack@caltech.edu

[2] Jet Propulsion Laboratory, Pasadena, CA 91109, USA

[3] Kavli Institute for Cosmological Physics, University of Chicago, 5640 South Ellis Avenue, Chicago, IL 60637, USA

[4] Department of Physics and Astronomy, University of Southern California, Los Angeles, CA 90089, USA

[5] Institute of Astronomy and Astrophysics, Academia Sinica, P.O. Box 23-141, Taipei 10617, Taiwan

[6] LeCosPA Center, National Taiwan University, Taipei 10617, Taiwan

Received 2012 September 21; accepted 2013 January 1; published 2013 February 1

ABSTRACT

We describe in detail our characterization of the compact radio source population in 140 GHz Bolocam observations of a set of 45 massive galaxy clusters. We use a combination of 1.4 and 30 GHz data to select a total of 28 probable cluster-member radio galaxies and also to predict their 140 GHz flux densities. All of these galaxies are steep-spectrum radio sources and they are found preferentially in the cool-core clusters within our sample. In particular, 11 of the 12 brightest cluster-member radio sources are associated with cool-core systems. Although none of the individual galaxies are robustly detected in the Bolocam data, the ensemble-average flux density at 140 GHz is consistent with, but slightly lower than, the extrapolation from lower frequencies assuming a constant spectral index. In addition, our data indicate an intrinsic scatter of $\simeq$30% around the power-law extrapolated flux densities at 140 GHz, although our data do not tightly constrain this scatter. For our cluster sample, which is composed of high-mass and moderate-redshift systems, we find that the maximum fractional change in the Sunyaev–Zel'dovich signal integrated over any single cluster due to the presence of these radio sources is $\simeq$20%, and only $\simeq 1/4$ of the clusters show a fractional change of more than 1%. The amount of contamination is strongly dependent on cluster morphology, and nearly all of the clusters with $\geqslant$1% contamination are cool-core systems. This result indicates that radio contamination is not significant compared with current noise levels in 140 GHz images of massive clusters and is in good agreement with the level of radio contamination found in previous results based on lower frequency data or simulations.

Key words: cosmology: observations – galaxies: clusters: general – radio continuum: galaxies

Online-only material: color figures

1. INTRODUCTION

Recently, large Sunyaev–Zel'dovich (SZ) effect surveys from the Atacama Cosmology Telescope (ACT), the South Pole Telescope (SPT), and *Planck* have delivered catalogs with hundreds of massive galaxy clusters (Sunyaev & Zel'dovich 1972; Vanderlinde et al. 2010; Marriage et al. 2011a; Reichardt et al. 2012b; *Planck* early results VIII: Planck Collaboration 2011a). In the case of ACT and SPT, which operate from the ground with modest frequency coverage near 150 GHz and arcminute resolution, unresolved galaxies present a potential systematic uncertainty in characterizing (or even detecting) galaxy clusters via the SZ effect (Cooray et al. 1998; Massardi & de Zotti 2004; Coble et al. 2007; Lin et al. 2009; Sehgal et al. 2010). Both instruments have accurately measured the blank-sky population of bright radio sources (Vieira et al. 2010; Marriage et al. 2011b) and the anisotropy power spectrum from both radio and dusty submillimeter sources (Das et al. 2011; Reichardt et al. 2012a). However, there are few observational constraints on the 150 GHz emission from member galaxies in massive clusters, even though clusters are known to host a significant number of radio galaxies. For example, within 0.5 arcmin of the cluster center there are $\simeq$30 times more radio sources compared to blank sky and from 0.5 to $\simeq$2 arcmin of the cluster center there are $\simeq$3 times more radio sources compared with blank sky (Coble et al. 2007; Muchovej et al. 2010). Unfortunately, the study of extragalactic radio sources at millimeter wavelengths is relatively immature, and it is therefore non-trivial to properly account for these radio sources in 150 GHz SZ data. Even worse, the bulk of the 150 GHz observational data is limited to very bright flat-spectrum sources and is not particularly relevant to the dimmer steep-spectrum sources typical of central cluster galaxies (Coble et al. 2007; Sadler et al. 2008; Vieira et al. 2010; Marriage et al. 2011b; Gold et al. 2011; Sajina et al. 2011; *Planck* early results XIII: Planck Collaboration 2011b).

Fortunately, the low-frequency properties of radio sources are well understood. First, radio sources are generally grouped into two families: flat spectrum and steep spectrum. Steep-spectrum sources have a $\simeq$1 GHz spectral index of $\alpha < -0.5$ and flat-spectrum sources have a $\simeq$1 GHz spectral index of $\alpha > -0.5$, where α describes a source spectrum of the form ν^{α} (de Zotti et al. 2010). Physically, a flat spectrum is typically due to synchrotron self-absorption (i.e., the medium is optically thick), which usually means the jet is oriented toward the viewer. In contrast, when the jet is orthogonal to the viewing angle, the optically thin lobes are visible, which tend to have a steep spectrum (de Zotti et al. 2010). For both families of radio sources, the spectral index tends to decrease at higher frequencies due to electron aging (relativistic energy loss) and/or the medium becoming less optically thick at higher frequencies (de Zotti et al. 2010; Kellermann 1966). This steepening has been observed in both flat-spectrum sources

[7] NASA Einstein Postdoctoral Fellow

(e.g., Sadler et al. 2008; Marriage et al. 2011b; Massardi et al. 2010; Planck Collaboration 2011b; Sajina et al. 2011) and steep-spectrum sources (e.g., Ricci et al. 2006; Tucci et al. 2011), although some measurements do not find such steepening (e.g., Lin et al. 2009; Vieira et al. 2010). In addition, steep-spectrum sources are generally associated with powerful elliptical and S0 galaxies (i.e., the bright cluster galaxy (BCG) of a massive cluster), and nearly all of the radio sources associated with clusters have a steep spectrum (e.g., Tucci et al. 2011; Coble et al. 2007). Finally, steep-spectrum sources tend to have little or no temporal variability (Tucci et al. 2011; Tingay et al. 2003; Sadler et al. 2006; Bolton et al. 2006). This wealth of knowledge has been exploited in a range of calculations and simulations to estimate the amount of radio contamination in 150 GHz SZ measurements (Lin et al. 2009; Sehgal et al. 2010; Andersson et al. 2011). These results indicate that radio contamination in massive clusters at 150 GHz should be relatively minor, but they have not yet been systematically verified via observational data.

2. DATA REDUCTION

2.1. Bolocam

During the period from 2006 to 2012, we observed a set of 45 massive galaxy clusters using Bolocam at the Caltech Submillimeter Observatory (Glenn et al. 1998; Haig et al. 2004; N. G. Czakon et al. 2013, in preparation; Sayers et al. 2012c). These clusters have a median mass of $M_{500} \simeq 9 \times 10^{14}\ M_{\odot}$ and masses as low as $M_{500} \simeq 3 \times 10^{14}\ M_{\odot}$, which is similar to the SPT and ACT mass limits (Marriage et al. 2011a; Reichardt et al. 2012b).[8] All of the masses were computed using *Chandra* X-ray data according to the methods described in Mantz et al. (2010). The median redshift of our sample is $z = 0.42$, and the median SZ signal-to-noise ratio (S/N) is 12. A complete description of these observations and data are given elsewhere (Sayers et al. 2011; N. G. Czakon et al. 2013, in preparation; Sayers et al. 2012c), and we briefly summarize the relevant details below. For all of these observations, Bolocam was configured to operate at 140 GHz,[9] with a 58 arcsec full-width at half-maximum (FWHM) point-spread function. All of the cluster images are 14×14 arcmin squares centered on the cluster. The centers of the images generally have noise RMSs of 0.7–1.5 mJy beam^{-1} (15–30 $\mu K_{\rm CMB}$ arcmin), increasing to approximately twice that value at the lower coverage edges of the images. This depth is similar to the SPT and ACT survey depths (Marriage et al. 2011a; Reichardt et al. 2012b).

In order to subtract atmospheric fluctuations from these data, we remove the time-instantaneous average signal over the field of view and then high pass filter the datastreams at a characteristic frequency of 250 mHz. This process also removes some astronomical signal from the data, and we quantify this via simulation to obtain a signal transfer function. For the results presented in this manuscript, the cluster signal transfer function was computed as described in detail in Sayers et al. (2011). We did not explicitly compute transfer functions for the point sources. Instead, we processed point-source models centered on the galaxy positions determined from low-frequency data through our reduction pipeline and then directly fit the resulting filtered image to our data. In all cases, the point-source models were normalized to an amplitude of 1 mJy. We note that the effective filtering of the point-source model is independent of the amplitude of the model for sources $\lesssim$100 Jy, which is at least 3 orders of magnitude brighter than any of the radio sources in our sample.

2.2. OVRO/BIMA and SZA

Most of our radio source flux densities at $\simeq$30 GHz were obtained from previously published results from the Owens Valley Radio Observatory (OVRO), the Berkeley–Illinois–Maryland Association (BIMA) array, and the Sunyaev–Zel'dovich Array (SZA; Coble et al. 2007; Bonamente et al. 2012). However, we reduced data collected by these facilities for an additional 13 radio sources (three from OVRO/BIMA and 10 from SZA). Our reduction of these previously unpublished data followed the methods described in, e.g., Coble et al. (2007) and Muchovej et al. (2007), and we refer the reader to those manuscripts for additional details. To obtain point-source flux densities, we simultaneously fit for the cluster SZ signal and all of the point sources. We modeled the cluster SZ emission using the best-fit generalized Navarro, Frenk, and White (gNFW) pressure profiles from Arnaud et al. (2010), which are described by

$$P(X) = \frac{P_0}{(C_{500}X)^{\gamma}[1 + (C_{500}X)^{\alpha}]^{(\beta-\gamma)/\alpha}}, \quad (1)$$

where P is the pressure, P_0 is the pressure normalization, X is the radial coordinate, C_{500} is the concentration parameter, and α, β, and γ describe the power-law slopes at moderate, large, and small radii. Corrections for the SZA primary beam were accounted for in both the cluster and point-source fits.

3. CLUSTER-MEMBER RADIO GALAXIES

3.1. Central Radio Galaxies–NVSS Selection

There are a significant number of bright radio galaxies near the centers of massive clusters (e.g., Coble et al. 2007 find that $\simeq$97% of radio sources within 0.5 arcmin of the cluster center are cluster members). Unfortunately, these sources are difficult to detect in our arcminute-resolution SZ data due to the large degeneracy between the inner slope of the SZ profile and the radio source flux density. Consequently, we have searched the 1.4 GHz NVSS catalog within 1 arcmin of each cluster center (Condon et al. 1998) in order to select probable cluster-member galaxies. We chose the NVSS survey for our galaxy selection because it has approximately uniform depth over the full sky above decl. $= -40$, and is complete above a flux density of 2.5 mJy. Throughout this paper we refer to the NVSS-selected sources within 1 arcmin as cluster-member galaxies. However, based on the results of Coble et al. (2007) and the blank-sky source density of the NVSS catalog, we expect $\gtrsim$5% of the sources to be field galaxies unassociated with the clusters.

Our search radius of 1 arcmin was chosen for two main reasons. First, the results of Coble et al. (2007) indicate that a 1 arcmin search radius is large enough to contain the bulk of the bright cluster-member radio galaxies without including a significant number of foreground and background galaxies

[8] M_{500} is the mass enclosed within a sphere with an average density of 500 times the background density.

[9] The SZ emission-weighted band center of Bolocam is 140.0 GHz. The effective band center for a typical radio source spectrum is slightly lower (138.7–139.2 GHz for the radio sources with $-1.5 \leqslant \alpha \leqslant -0.5$). This difference in effective band center produces less than a 1% change in the extrapolated flux density from 30 GHz, and is therefore not included in our analysis. Furthermore, we note that our data are calibrated against objects with an approximately thermal spectrum, and both the source spectrum and the Bolocam spectral response were fully accounted for in the calibration (Sayers et al. 2012b).

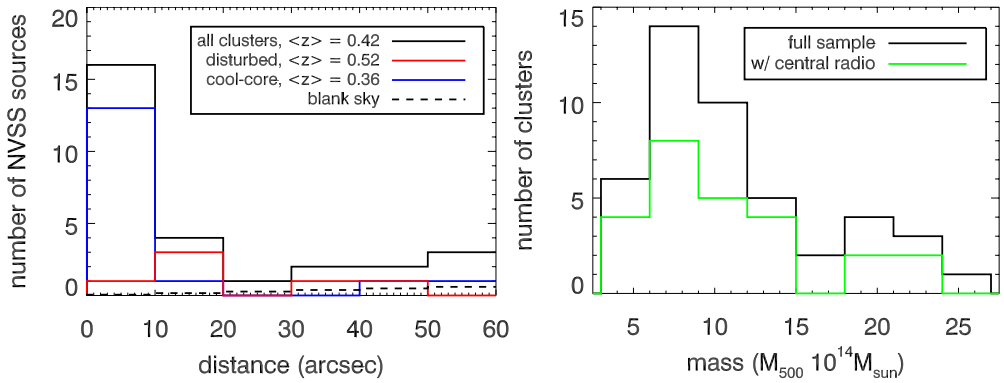

Figure 1. Left: the number of NVSS sources as a function of radius from the cluster centers. We show the number of NVSS sources for the full sample of 45 clusters, the 16 disturbed clusters, and the 17 cool-core clusters. Note the significant number of NVSS sources at the very center of cool-core clusters. For reference, we also show the blank-sky average number of sources for the NVSS survey given the angular size of each bin. Right: cluster masses for both the full sample of 45 objects and for the subset of 25 objects with central radio sources. The masses were computed from *Chandra* X-ray data according to the methods described in Mantz et al. (2010).

(A color version of this figure is available in the online journal.)

that are not associated with the cluster (see Figure 1). Second, by choosing a search radius approximately equal to our beam FWHM we include all of the galaxies that will not be resolved separately from the cluster SZ peak. Our choice of a fixed angular search radius means that the search radius in physical distance (e.g., kpc) varies significantly over our sample, which could produce biases in our galaxy selection. However, given that the number of NVSS sources falls dramatically beyond $\simeq$10 arcsec in radius, it is unlikely that a significant number of bright cluster-member galaxies will fall outside of our search radius. Furthermore, as justified above, our search radius is small enough such that the contamination from non-cluster galaxies is expected to be small. Therefore, we do not expect any significant biases in our galaxy selection due to our choice of search radius.

Over our sample of 45 clusters, we find 31 NVSS sources spread between 26 clusters (three clusters contain two sources and one cluster contains three sources, see Table 1). In agreement with previous results (e.g., Mittal et al. 2009), most of our cool-core clusters have at least one compact NVSS source (15/17), while less than half of the disturbed clusters in our sample have a compact NVSS source (6/16). Note that our classification of clusters as cool core or disturbed is based on X-ray measurements and is described in detail in Sayers et al. (2012c). Briefly, the projected luminosity ratio ($L_{\rm rat} = L(R < 0.05R_{500})/L(R < R_{500})$) is used to define cool-core systems (Mantz 2009; Mantz et al. 2010; Böhringer et al. 2010), with clusters having $L_{\rm rat} > 0.17$ classified as cool cores. The centroid shift parameter (w_{500}), which measures the difference between the X-ray peak and the X-ray centroid as a function of radius, is used to define disturbed systems (Maughan et al. 2008; Pratt et al. 2009; Maughan et al. 2012), with clusters having $w_{500} \geqslant 0.01$ classified as disturbed. We note that two systems are both cool core and disturbed, so the number of non-cool-core disturbed systems with compact NVSS sources is 4/14.

3.2. Central Radio Galaxies–140 GHz Properties

For each of these NVSS-selected sources, we have measured the 140 GHz flux density as follows. First, we jointly fit a point-source template centered on the NVSS coordinates, along with a template for the SZ emission, to our data. Our fitting procedure is described in detail in Sayers et al. (2011), and we refer the reader to that manuscript for additional details. The normalization of the point-source template gives the flux density of the source (in mJy). For the SZ template, we used the morphology-dependent best-fit gNFW pressure profiles from Arnaud et al. (2010; e.g., we used the best-fit cool-core template for the cool-core clusters in our sample), allowing the normalization of the template (i.e., P_0) to be a free parameter. These profiles were used because all of the point sources we fit are in the central regions of the cluster, where the shape of the pressure profiles varies significantly with morphological type. We then inserted the best-fit SZ and point-source templates into 100 noise realizations and repeated the fit in order to characterize our uncertainty on the point-source flux density. For most of our data, the raw point-source sensitivity is $\simeq$1 mJy, but our uncertainties on the flux densities of these point sources are $\simeq$1–3 mJy, with the degradation due to degeneracies between the SZ and point-source templates. The sensitivity degradation depends strongly on the separation of the SZ and point-source centroids, along with the angular size of the SZ template. For clusters with multiple radio sources, we fit for each source separately. The best-fit flux densities are given in Table 2.

We then derived an independent estimate for the 140 GHz flux densities of the sources by extrapolating the low-frequency data. We have primarily combined 1.4 GHz NVSS data with $\simeq$30 GHz measurements from SZA and/or OVRO/BIMA, which exist for 24/28 sources (Bonamente et al. 2012; Coble et al. 2007).[10] Three of the sources without 30 GHz data have measurements at either 4.85 GHz and/or frequencies below 1.4 GHz, which have been used to constrain the spectral energy distributions (SEDs) of those sources (Cohen et al. 2007; Large et al. 1981; Griffith et al. 1994). We fit an SED of the form $\nu^{\alpha_{1.4/30}}$, and we find all of the galaxies have $\alpha_{1.4/30} < -0.50$ (see Figure 2). Our fits include both the measurement uncertainties and overall flux calibration uncertainties on the source flux densities, the latter of which is equal to 3% for the NVSS measurements, 4% for the OVRO/BIMA measurements, and 5% for SZA measurements (Condon et al. 1998; Reese et al. 2002; Muchovej et al. 2007). We note that there are some systematic differences in calibration between the data sets (e.g., using pre- or post-WMAP planetary models), but these differences are below the flux calibration

[10] Three out of thirtyone of the NVSS sources are extended and appear to have very steep spectral indices. Extrapolating to 140 GHz, we expect negligible flux density from these three sources and therefore have not attempted to fit to them in our data.

Table 1
NVSS Sources within 1 arcmin of the Cluster Center

Cluster	Redshift	Morphology		NVSS Sources			
		Cool Core	Disturbed	R.A. (J2000)	Decl. (J2000)	Distance (arcsec)	1.4 GHz Flux Density (mJy)
MACS J0018.5	0.54					No sources	
MACS J0025.4	0.58			00:25:32.0	−12:23:09.1	39	28.7 ± 1.3
ZWCL 0024	0.39		✓	00:26:35.5	+17:09:31.7	10	2.6 ± 0.4
A209	0.21			01:31:52.7	−13:36:59.6	13	18.4 ± 1.0
CL J0152.7	0.83		✓			No sources	
A267	0.23		✓			No sources	
A370	0.38		✓	02:39:55.3	−01:34:18.3	37	10.5 ± 1.0
A383	0.19	✓		02:48:03.4	−03:31:43.9	3	40.9 ± 1.3
MACS J0257.1	0.50					No sources	
MACS J0329.6	0.45	✓	✓	03:29:41.7	−02:11:52.2	7	6.9 ± 0.6
MACS J0416.1	0.42		✓			No sources	
MACS J0417.5	0.44	✓	✓	04:17:34.9	−11:54:34.2	12	29.8 ± 1.7
MACS J0429.6	0.40	✓		04:29:36.0	−02:53:06.4	0	138.8 ± 4.2
MACS J0451.9	0.43		✓			No sources	
MACS J0454.1	0.55		✓			No sources	
MACS J0647.7	0.59					No sources	
MACS J0717.5	0.55		✓	07:17:34.1	+37:45:01.3	31	90.9 ± 3.7
				07:17:35.7	+37:45:39.2	47	102.5 ± 3.7
MACS J0744.8	0.69		✓			No sources	
A611	0.29					No sources	
A697	0.28					No sources	
MACS J0911.2	0.50					No sources	
A963	0.21					No sources	
MS 1054	0.83		✓	10:56:59.6	−03:37:26.8	18	14.1 ± 0.9
MACS J1115.8	0.36	✓		11:15:51.8	+01:29:55.5	2	16.2 ± 1.0
MACS J1149.5	0.54		✓			No sources	
A1423	0.21			11:57:16.8	+33:36:44.6	9	33.3 ± 0.9
MACS J1206.2	0.44			12:06:12.1	−08:48:02.5	4	160.9 ± 6.3
CL J1226	0.89			12:26:58.3	+33:32:44.3	7	4.3 ± 0.5
MACS J1311.0	0.49	✓				No sources	
MACS J1347.5	0.45	✓		13:47:30.1	−11:45:30.2	23	17.7 ± 3.2
				13:47:30.7	−11:45:08.6	2	45.9 ± 1.5
A1835	0.25	✓		14:01:02.1	+02:52:41.0	2	39.3 ± 1.6
MACS J1423.8	0.55	✓		14:23:47.9	+24:04:39.9	3	8.0 ± 1.1
MACS J1532.9	0.36	✓		15:32:53.8	+30:20:59.8	1	22.8 ± 0.8
A2204	0.15	✓		16:32:46.9	+05:34:34.9	5	69.3 ± 2.5
A2219	0.23			16:40:15.0	+46:42:28.7	55	6.1 ± 0.5
				16:40:21.8	+46:42:47.8	24	239.1 ± 8.3
				16:40:23.8	+46:41:47.3	56	7.9 ± 1.0
MACS J1720.3	0.39	✓		17:20:15.3	+35:35:26.3	59	9.6 ± 0.5
				17:20:16.8	+35:36:28.4	6	18.0 ± 1.0
A2261	0.22	✓		17:22:27.7	+32:07:57.8	8	5.3 ± 0.5
MACS J1931.8	0.35	✓		19:31:49.9	−26:35:13.4	40	216.5 ± 6.9
MS 2053	0.58		✓			No sources	
MACS J2129.4	0.59		✓			No sources	
RX J2129.6	0.24	✓		21:29:40.0	+00:05:23.0	7	25.4 ± 1.2
MS 2137	0.31	✓		21:40:15.0	−23:39:39.5	2	3.8 ± 0.5
MACS J2211.7	0.40	✓				No sources	
MACS J2214.9	0.50		✓	22:14:56.5	−14:00:55.7	46	5.6 ± 0.6
AS1063[a]	0.35					No sources	

Notes. NVSS sources within 1 arcmin of the cluster center for the 45 clusters in our sample. The columns give the cluster name, the cluster redshift, the X-ray morphology, the R.A./decl. of the NVSS source, the distance from the cluster center to the NVSS source, and the NVSS flux density at 1.4 GHz. The superscript "a" denotes that AS1063 is below the declination range of the NVSS survey (−40 deg), and we therefore searched the SUMSS catalog instead (Bock et al. 1999; Mauch et al. 2003; Murphy et al. 2007). The SUMSS survey is similar in depth to the NVSS survey, although at lower frequency. We found no SUMSS sources within 1 arcmin of the center of AS1063.

uncertainties quoted for each data set. Furthermore, for our SED fits we assume a single observing frequency for each data set independent of source spectrum. This results in a negligible bias in our results due to the small fractional bandwidths and large separations in band centers among our data sets (1.4, 30, and 140 GHz).

Although our source selection using 1.4 GHz data favors steep-spectrum sources, we note that the ≃30 GHz data do not contain any point-source detections without an NVSS counterpart. The ≃30 GHz data are generally sensitive to sources with flux densities larger than 0.5–1.0 mJy, and would therefore have detected bright flat-spectrum sources if they

Table 2
Central Radio Sources

Cluster	NVSS 1.4 GHz mJy	OVRO/BIMA 28.5 GHz mJy	SZA 30.9 GHz mJy	$\alpha_{1.4/30}$	Extrap. 140 GHz mJy	Bolocam 140 GHz mJy
MACS J0025.4	28.7 ± 1.3	0.33 ± 0.17[c]		-1.38	0.06 ± 0.05	-2.3 ± 2.0
ZWCL 0024	2.6 ± 0.4		-0.2 ± 0.2	-1.09	0.01 ± 0.02	0.6 ± 5.3
A209	18.4 ± 1.0		1.1 ± 0.2	-0.91	0.28 ± 0.07	-1.2 ± 2.1
A370	10.5 ± 1.0	0.72 ± 0.09[c]	0.8 ± 0.2	-0.88	0.18 ± 0.03	-3.4 ± 1.8
A383	40.9 ± 1.3	4.40 ± 0.50[a]	4.3 ± 0.3[b]	-0.73	1.41 ± 0.14	5.4 ± 2.1
MACS J0329.6	6.9 ± 0.6		0.3 ± 0.4	-1.04[d]	0.10 ± 0.12	3.9 ± 3.1
MACS J0417.5	29.8 ± 1.7			-1.11[d]	0.18 ± 0.03	2.3 ± 2.1
MACS J0429.6	138.8 ± 4.2		18.2 ± 0.9[b]	-0.66	6.70 ± 0.50	9.8 ± 3.5
MS 1054	14.1 ± 0.9	0.94 ± 0.07[a]		-0.90	0.22 ± 0.03	1.6 ± 1.7
MACS J1115.8	16.2 ± 1.0		1.4 ± 0.4[b]	-0.81	0.42 ± 0.18	-2.7 ± 1.9
A1423	33.3 ± 0.9		0.6 ± 0.2	-1.31	0.09 ± 0.04	-3.5 ± 2.8
MACS J1206.2	160.9 ± 6.3			-1.38[d]	0.27 ± 0.08	-5.4 ± 1.9
CL J1226	4.3 ± 0.5		0.3 ± 0.2	-0.92	0.09 ± 0.08	1.3 ± 3.3
MACS J1347.5	45.9 ± 1.5	10.38 ± 0.47[a]	8.7 ± 0.5[b]	-0.51	4.39 ± 0.21[e]	-4.4 ± 1.8
A1835	39.3 ± 1.6	2.97 ± 0.13[a]	2.9 ± 0.3[b]	-0.85	0.77 ± 0.05	-1.1 ± 1.4
MACS J1423.8	8.0 ± 1.1	1.49 ± 0.13[a]	2.0 ± 0.2[b]	-0.50	0.76 ± 0.10	2.1 ± 2.8
MACS J1532.9	22.8 ± 0.8	3.25 ± 0.22[a]	3.2 ± 0.3[b]	-0.64	1.19 ± 0.10	2.5 ± 2.7
A2204	69.3 ± 2.5	8.79 ± 0.37[a]	7.0 ± 0.4[b]	-0.71	2.65 ± 0.16	1.1 ± 1.4
A2219	6.1 ± 0.5		0.6 ± 0.2	-0.74	0.21 ± 0.09	4.9 ± 2.6
	239.1 ± 8.3	14.87 ± 0.62[a]	14.2 ± 0.7	-0.92	3.43 ± 0.17	-4.9 ± 3.3
	7.9 ± 1.0		0.1 ± 0.1	-1.40	0.02 ± 0.02	-7.3 ± 2.4
MACS J1720.3	9.6 ± 0.5		0.6 ± 0.1	-0.90	0.15 ± 0.04	5.3 ± 1.6
	18.0 ± 1.0		1.8 ± 0.4[b]	-0.76	0.58 ± 0.21	-5.1 ± 2.4
A2261	5.3 ± 0.5	0.20 ± 0.30		-1.10	0.05 ± 0.07	-4.8 ± 1.3
MACS J1931.8	216.5 ± 6.9			-0.72[d]	8.81 ± 4.56	-3.0 ± 2.2
RX J2129.6	25.4 ± 1.2	2.33 ± 0.14[a]	2.6 ± 0.2[b]	-0.77	0.71 ± 0.06	0.1 ± 2.9
MS 2137	3.8 ± 0.5			N/A	0.06[f]	-7.5 ± 5.1
MACS J2214.9	5.6 ± 0.6		0.4 ± 0.3	-0.89	0.14 ± 0.13	-2.8 ± 2.3

Notes. Compact central radio sources in our sample of 45 clusters. The columns give the cluster name, the NVSS flux density at 1.4 GHz, the OVRO/BIMA flux density at 28.5 GHz, the SZA flux density at 30.9 GHz, the spectral index determined from the 1.4 and $\simeq$30 GHz data, the predicted flux density at 140 GHz based on that spectral index, and the measured flux density in our 140 GHz image at the location of the source, which is in some cases negative due to noise fluctuations. All of the uncertainties are 1σ values and include flux calibration uncertainties; the Bolocam uncertainties are approximately Gaussian and include degeneracies between the point source and the cluster SZ signal (see the text). Superscripts denote the following: [a]measurements from Coble et al. (2007); [b]measurements from Bonamente et al. (2012); [c]sources published in Coble et al. (2007), but refit in our analysis (the source associated with MACS J0025.4 was published in B1950 coordinates in Coble et al. 2007); [d]spectral index based on fits with 4.85 GHz and/or lower frequency data (Cohen et al. 2007; Large et al. 1981; Griffith et al. 1994); [e]source detected by two groups at millimeter/submillimeter frequencies, and the best-fit 140 GHz flux density from the combination of those data and the radio results is 4.4 ± 0.3 mJy (Pointecouteau et al. 2001) and 5.5 ± 0.6 mJy (Komatsu et al. 1999), consistent with our extrapolated estimate; [f]only 1.4 GHz data were available for this source, so it was extrapolated based on the median value of $\alpha_{1.4/30}$ for our sample (-0.89). We note that some of the extrapolated flux densities are consistent with 0. We quote symmetric uncertainties about these best-fit values, even though the true probability density functions are asymmetric and exclude unphysical negative values.

exist in the central regions of these clusters. Since all of the bright central radio sources are steep-spectrum sources, which tend to have little or no temporal variability (Tingay et al. 2003; Sadler et al. 2006; Bolton et al. 2006), the asynchronous NVSS/SZA/OVRO/BIMA observations should provide an accurate characterization of the source SED. We used the values of $\alpha_{1.4/30}$ to predict the flux density at 140 GHz, and these extrapolated values are given in Table 2.

None of the NVSS sources near cluster centers are detected at a significant level in our 140 GHz images ($>3\sigma$). Consequently, we have characterized the average point-source signal measured in our data by comparing our measured flux density to the predicted flux density based on the extrapolation from lower frequency measurements. To avoid correlations and biases in this average measurement, we have discarded the data from clusters with multiple NVSS sources, those with no 30 GHz data, and also A2261 due to the fact that the SZ template does not provide a good description of those data. For the 17 remaining clusters we formed the quantity

$$\delta = \frac{S_{\rm Bolo} - S_{\rm extrap}}{\sqrt{\sigma^2(S_{\rm Bolo}) + \sigma^2(S_{\rm extrap})}},$$

where $S_{\rm Bolo}$ is the best-fit flux density in our Bolocam image, $S_{\rm extrap}$ is the extrapolated flux density based on the lower frequency measurements assuming a constant spectral index, $\sigma(S_{\rm Bolo})$ is the uncertainty on the Bolocam measurement, and $\sigma(S_{\rm extrap})$ is the uncertainty on the extrapolated flux density.

If our extrapolation of the spectral index found at lower frequencies perfectly describes our data then the values of δ will have a mean of 0 and standard deviation of 1. We find a mean $\delta = -0.26 \pm 0.28$, which indicates that our data show no statistically significant evidence for a change in the spectral index above 30 GHz, although our data are consistent with a slight steepening

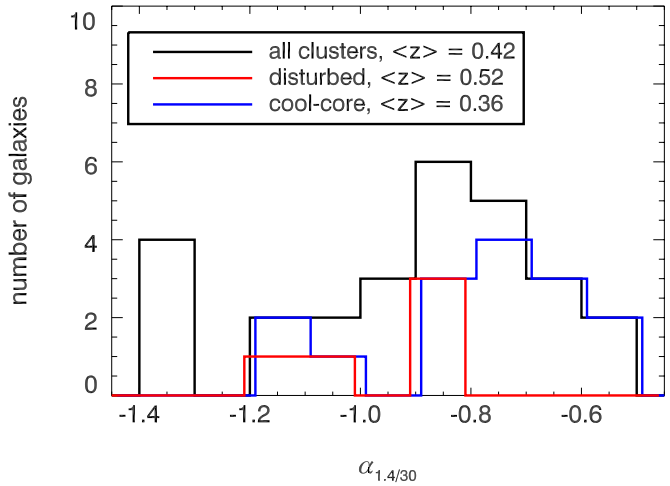

Figure 2. Value of the spectral index $\alpha_{1.4/30}$ found for the cluster-member galaxies in our sample using measurements at $\nu \leqslant 30$ GHz. All of these galaxies are steep-spectrum sources, and we find a median spectral index of -0.89. The spectral indices for the disturbed and cool-core sub-samples are also shown, and have been offset by 0.01 for ease of viewing. Compared with the full sample, the galaxies associated with cool-core clusters have shallower spectral indices on average.

(A color version of this figure is available in the online journal.)

of the spectral index (a steepening is consistent with previous results and theoretical expectations: Tucci et al. 2011; Ricci et al. 2006; Kellermann 1966). Furthermore, we note that a one-sample Kolmogorov–Smirnov goodness-of-fit test shows that our values of δ are consistent with a Gaussian distribution with a probability to exceed of 0.60. In addition, we directly computed the standard deviation of the 17 values of δ, and we find that this standard deviation is StdDev(δ) $= 1.14 \pm 0.18$. This value is consistent with 1, which is the expectation under the assumption that the dispersion in the values of δ is due entirely to measurement noise. However, if we assume there is an intrinsic scatter $\sigma_{\rm int}$ in the true 140 GHz flux densities compared with the extrapolated 140 GHz flux densities, then

$$\mathrm{StdDev}(\delta) = \sqrt{1 + \sigma_{\rm int}^2},$$

and our data imply a best-fit intrinsic scatter of $\simeq$30%.

We also examined whether the Bolocam data show a significant detection of the ensemble-average flux density of these radio sources, again focusing on the same subset of 17 objects. Analogous to the quantity δ, we formed the quantity

$$\mathrm{SN}_{\rm Bolo} = \frac{S_{\rm Bolo}}{\sigma(S_{\rm Bolo})}.$$

We find a mean $\mathrm{SN}_{\rm Bolo} = 0.14 \pm 0.24$, indicating that our 140 GHz data do not show statistically significant evidence for the presence of these radio sources. However, if we focus solely on the brightest sources with $S_{\rm extrap} > 1$ mJy, then we find a mean $\mathrm{SN}_{\rm Bolo} = 1.76 \pm 0.50$, showing a detection of these sources at modest statistical significance ($\simeq 3.5\sigma$). This implies that our non-detection of the ensemble average of all radio sources is likely due to the fact that most of the sources are well below the Bolocam noise RMS, which means that averaging over these sources adds a significant amount of noise but very little signal. For completeness, we note that the mean value of δ for these brightest sources is 0.54 ± 0.62, which is also consistent with no change in the spectral index between 30 GHz and 140 GHz.

3.3. Central Radio Galaxies–SZ Contamination

Since the extrapolation of the radio galaxy flux densities from lower frequencies provides a good description of our 140 GHz data, we subtracted each of the radio galaxies using the extrapolated flux density. A complete list of the subtracted radio sources is given in Table 3. In most cases, the measurement uncertainty on the extrapolated flux density is quite small, and our overall uncertainty is therefore dominated by the 30% intrinsic scatter in the extrapolation. We then computed the peak SZ S/N for each cluster both with and without the radio source(s) subtracted using the optimal filtering formalism described in Sayers et al. (2012a). Briefly, we construct an SZ template of the form $S(\theta) \propto (1 + \theta^2/\theta_c^2)^{-1}$, weight this template by the signal transfer function of our map and the inverse of the map variance, convolve our map with the resulting filter, and search for the peak S/N. This is repeated for $\theta_c = 0.25, 0.50, \ldots, 3.00$, and the maximum peak S/N over all filter scales is used to describe the SZ S/N. This is essentially the same algorithm used by both ACT and SPT to search for clusters in their survey data (Vanderlinde et al. 2010; Marriage et al. 2011a; Reichardt et al. 2012b). We find the maximum fractional change in SZ S/N for any of the clusters is $\simeq$20%, and only 13/45 of the clusters show a fractional change in SZ S/N larger than 1% (see Figure 3). Consequently, for the high-mass and moderate-redshift clusters in our sample contamination from radio emission is in general small compared with the noise in our data. Furthermore, for the brightest radio galaxies, we generally find that the value of θ_c with the maximum SZ S/N is smaller when the radio source is subtracted from the map, which is due to the resulting cluster profile being more sharply peaked (recall that these radio sources partially fill in the SZ decrement at 140 GHz).

Although the overall level of radio contamination in our sample is small, we note that 11/12 of the brightest radio sources are associated with cool-core systems, and therefore 11/17 cool-core systems show a fractional change in SZ S/N larger than 1%.[11] Previous studies have found a similar relationship between strong radio emission and cool-core systems (e.g., Sun 2009). Further supporting this trend of cool-core systems hosting the brightest radio galaxies, we also find a correlation between the strength of the radio emission and the projected X-ray luminosity ratio, which we have used to separate cool-core and non-cool-core systems (see Figure 3). This correlation is quantified by a Spearman rank coefficient of 0.46 and null hypothesis probability of 0.02 (for 25 data points). In addition, we find that there is no significant correlation between the fractional change in SZ S/N and cluster mass for our sample, quantified by a Spearman rank coefficient of -0.11 and a null hypothesis probability of 0.59 (again for 25 data points, see Figure 3). Consequently, the fractional change in SZ S/N due to radio contamination is approximately independent of mass for these high-mass systems. Since there is no evidence for a correlation between cluster mass and fractional change in SZ S/N, and since our sample approximately spans the mass range of objects discovered by the ACT and SPT surveys (Marriage et al. 2011a; Reichardt et al. 2012b), the amount of radio contamination in those surveys should be similar to what we have

[11] The median redshift of the cool-core systems in our sample ($z = 0.36$) is slightly lower than the median redshift of the full sample ($z = 0.42$) and the median redshift of the disturbed systems ($z = 0.52$). Consequently, some of the difference in radio contamination for the different morphological classifications may be due to these differences in redshift rather than the cluster environment.

Table 3
Compact Central Radio Sources

Cluster	Subtracted PS (mJy)	SZ S/N (raw)	θ_c (raw) (arcmin)	SZ S/N (PS-sub)	θ_c (PS-sub) (arcmin)	Δ S/N (%)
MACS J0025.4	0.06	12.31	0.50	12.33	0.50	0.2
ZWCL 0024	0.01	3.26	3.00	3.26	3.00	0.0
A209	0.28	13.93	1.75	14.00	1.50	0.5
A370	0.18	12.80	0.50	12.89	0.50	0.7
A383[a]	1.41	9.33	2.00	9.72	2.00	4.2
MACS J0329.6	0.10	12.09	0.25	12.13	0.25	0.3
MACS J0417.5	0.18	22.67	1.00	22.71	1.00	0.2
MACS J0429.6	6.70	7.34	1.50	9.09	1.00	23.8
MS 1054	0.22	17.38	0.50	17.55	0.50	1.0
MACS J1115.8	0.42	10.92	1.25	11.05	1.25	1.2
A1423	0.09	5.80	0.50	5.82	0.50	0.3
MACS J1206.2	0.27	21.69	1.00	21.80	1.00	0.5
CL J1226	0.09	13.01	0.25	13.05	0.25	0.3
MACS J1347.5	4.39	34.04	0.50	36.90	0.25	8.4
A1835	0.77	15.34	0.75	15.76	0.50	2.8
MACS J1423.8	0.76	8.98	0.50	9.39	0.50	4.6
MACS J1532.9	1.19	7.55	0.75	8.04	0.50	6.5
A2204	2.65	20.94	1.00	22.41	0.75	7.0
A2219	3.43	10.53	1.00	11.12	1.00	5.6
	0.21					
	0.02					
MACS J1720.3	0.58	10.32	0.25	10.67	0.25	3.4
	0.15					
A2261[a]	0.05	10.76	0.25	10.79	0.25	0.3
MACS J1931.8	8.81	9.21	1.25	10.20	1.00	10.8
RX J2129.6	0.71	7.76	0.75	8.02	0.75	3.4
MS 2137	0.06	6.51	0.25	6.53	0.25	0.3
MACS J2214.9[a]	0.14	12.85	1.00	12.86	1.00	0.1

Notes. Compact central radio sources subtracted from Bolocam cluster data based on extrapolations from lower frequencies. From left to right the columns give: the flux density of the subtracted radio source, the SZ S/N in our unsubtracted image, the filter scale corresponding to this peak SZ S/N in our unsubtracted image, the SZ S/N in our point-source-subtracted image, the filter scale corresponding to the peak SZ S/N in our point-source-subtracted image, and the fractional difference in SZ S/N between the unsubtracted and point-source-subtracted images. In general, the extrapolated flux densities of the radio sources are accurate to ≃30%, limited by the intrinsic scatter in the extrapolation. Consequently, the fractional change in the SZ S/N is also accurate to ≃30%. The superscript "a" denotes clusters that contain point sources directly detected in our Bolocam images away from the cluster centers (see Section 5). These additional point sources were not subtracted for this analysis.

found for our sample. However, we caution that those surveys contain a significantly larger fraction of low-mass clusters, and the negative Spearman rank coefficient indicates that our data favor an on-average increase in fractional change in SZ S/N with decreasing cluster mass (although at low significance given the 59% probability of our data being consistent with no trend in mass).

Due to the way we have selected the cluster-member radio sources, anything below the NVSS detection limit (2.5 mJy at 1.4 GHz) will not be included in our analysis. However, even if we assume the smallest magnitude spectral index found for any of the radio galaxies in our sample ($\alpha_{1.4/30} = -0.50$), a source undetected by NVSS would have a maximum 140 GHz flux density of 0.25 mJy. Therefore, it is unlikely that a source undetected by NVSS would have more than a 1% effect on the optimally filtered peak SZ signal we measure for any of the clusters in the Bolocam sample. We do note that, of the 21 central radio sources detected by Coble et al. (2007), there were two sources with spectral indices smaller in magnitude than $\alpha_{1.4/30} = -0.5$, and one source with a spectral index of $\alpha_{1.4/30} = -0.14$. Since our ≃30 GHz data are most sensitive to these flat-spectrum sources, we consider the extreme case of a source with $\alpha_{1.4/30} = -0.14$ and a ≃30 GHz flux density just below our detection limit of $\lesssim$1 mJy. Such a source could go undetected in our ≃30 GHz data and still have a 140 GHz flux density of ≃0.5 mJy. Such a source would likely produce a ≃1% change in the SZ S/N measured by Bolocam (see Figure 3). However, given the rarity of such flat-spectrum sources in the centers of clusters, coupled with the fact that the source would also need to be close to our detection threshold, it is unlikely that there are a significant number of such sources in the Bolocam cluster sample.

3.4. Non-central Cluster-member Radio Galaxies

Although the number of cluster radio galaxies drops quickly with radius, there are likely to be some cluster-member radio galaxies outside of our 1 arcmin diameter search radius. For example, the total number of radio sources in the central ≃2 arcmin radius of our images is enhanced by a factor of ≃3 compared with the blank-sky average (Coble et al. 2007; Muchovej et al. 2010). However, there are significantly fewer sources in these regions compared with the cluster centers (a factor of ≃10), and the contamination from these sources will be much less degenerate with the cluster SZ signal due to the relatively large spatial separation. Therefore, we expect the contamination from these sources to be significantly

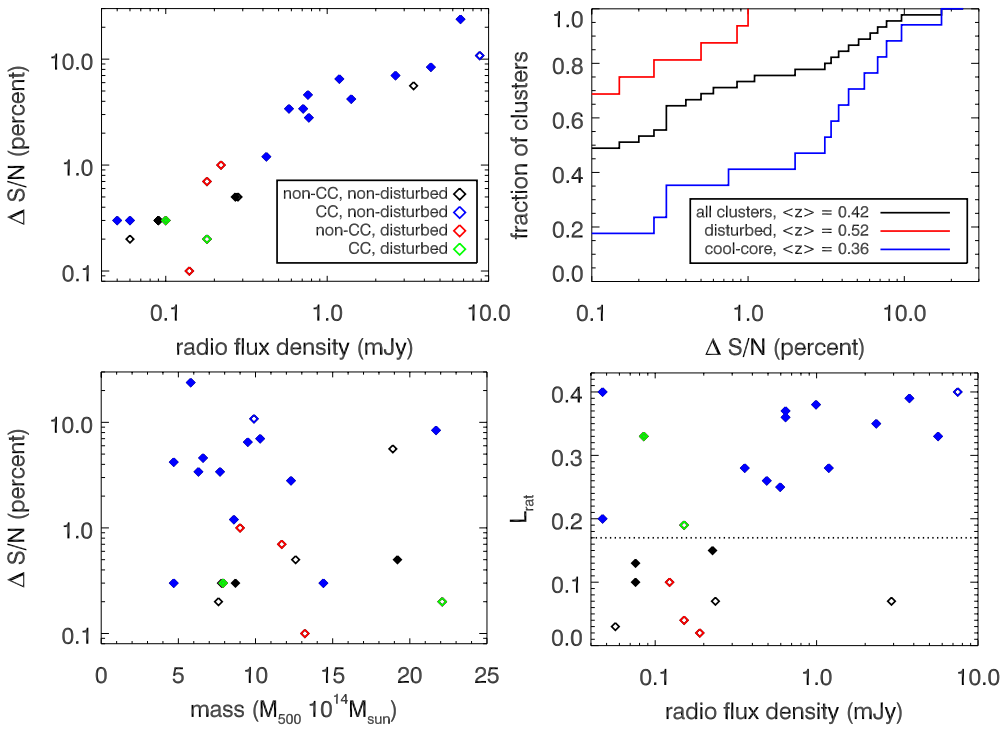

Figure 3. Top left: the fractional change in the SZ S/N as a function of the extrapolated 140 GHz flux density of the radio source. The maximum change is $\simeq$20% and a flux density $\gtrsim$0.5 mJy is required to produce more than a 1% change in SZ S/N. The data are color-coded by X-ray-derived morphology, and nearly all of the brightest radio sources are associated with cool-core systems. Over half of the radio sources are within 10 arcsec of the cluster center (25–75 kpc for the redshift range of our sample), and these sources are marked as filled symbols. Note that roughly half the clusters in our sample contain no radio sources given our selection criteria, and are therefore not included in this plot. Top right: the cumulative fraction of clusters with radio contamination below a given threshold (as quantified by fractional change in SZ S/N). The black, red, and blue curves represent the full sample of 45 clusters, the disturbed sub-sample, and the cool-core sub-sample, respectively. The radio contamination is severe enough to cause a >1% change in the SZ signal for $\simeq$25% of the clusters in our sample, although the contamination is significantly worse in cool-core systems. Note that the cumulative fraction ignores sources undetected by NVSS, and is therefore likely to be an overestimate at Δ S/N $\lesssim$ 1%. Bottom left: the fractional change in SZ S/N vs. cluster mass, showing no evidence for a correlation and indicating that the fractional amount of radio contamination is approximately independent of mass for these high-mass clusters. Bottom right: the X-ray-projected luminosity ratio $L_{\rm rat} = L(R < 0.05R_{500})/L(R < R_{500})$ vs. the 140 GHz flux density of the radio source, which shows a correlation and indicates that the brightest radio sources are preferentially found in the clusters with the largest projected luminosity ratio. We define cool-core systems as clusters with $L_{\rm rat} \geqslant 0.17$ (Mantz 2009).

(A color version of this figure is available in the online journal.)

smaller than the contamination from the central radio galaxies. Consequently, we examine the effects of these sources in a statistical sense.

First, the factor of three increase in the number of radio sources will increase the corresponding noise fluctuations from undetected sources by a factor of $\simeq\sqrt{3}$. However, even with this enhancement the noise fluctuations from radio sources will still be sub-dominant to the noise fluctuations from dusty star-forming galaxies and negligible compared with the noise RMS in our images ($\lesssim$0.1 mJy compared with $\simeq$1 mJy). Furthermore, we note that the increased number of radio sources in the direction of the cluster will systematically fill in the SZ decrement, which is referenced to the average signal level outside of the cluster, and bias our results. Based on a simple power-law extrapolation of the measured number counts at $\simeq$140 GHz,[12] which constrain the number counts above $\simeq$10 mJy, we estimate that the SZ decrement will be filled in by $\simeq$0.01 mJy arcmin^{-2} due to the higher than average number of radio sources toward the cluster (Vieira et al. 2010; Marriage et al. 2011b; Planck Collaboration 2011b). This surface brightness is almost 3 orders of magnitude below the average SZ surface brightness toward the clusters in our sample and therefore should produce a $\simeq$0.1% bias in the average SZ signal recovered. Consequently, contamination from radio galaxies outside of 1 arcmin in radius from the cluster center should generally be negligible.

[12] Measurements at a wide range of frequencies indicate that a simple power law is a good approximation of the number counts on the low-flux side of the break in the counts (e.g., Tucci et al. 2011).

4. POSSIBLE CONTAMINATION FROM DUSTY GALAXIES

In addition to radio emission, some of the cluster-member galaxies are likely to have thermal dust emission. Studies of clusters out to $z = 0.8$ in the mid-IR with *Spitzer* have shown that there can be significant enhancements in the number of 24 μm-detected sources within narrow redshift slices centered on clusters (Bai et al. 2007; Marcillac et al. 2007). However, the total number of 24 μm objects detected toward clusters is $\lesssim$10% above the number detected toward blank fields at similar sensitivities, due to the fact that the sources are detected over a wide range of redshifts (Geach et al. 2006; Finn et al. 2010). Compared with 24 μm observations, our data are significantly more sensitive to high-redshift galaxies and less sensitive to dust emission from cluster-member galaxies (Blain et al. 2002; Béthermin et al. 2011), and so the effective enhancement compared to a blank field will be even smaller in our Bolocam images. Furthermore, *Herschel* has recently published results characterizing the dust emission from 68 cluster BCGs at frequencies as low as 600 GHz (Rawle et al. 2012). Fifteen

Table 4
Point Sources Detected by Bolocam

Cluster	Coordinates J2000	Radius (arcmin)	NVSS 1.4 GHz	OVRO/BIMA 28.5 GHz	SZA 30.9 GHz	Bolocam 140 GHz	SZ S/N (raw)	SZ S/N (PS-sub)
A267	01:52:54.6, +01:02:08.2	3.51	4.6 ± 0.5	7.55 ± 0.24		9.8 ± 2.3	9.83	9.57
A383	02:48:22.1, −03:34:30.5	5.44	54.9 ± 2.4		7.5 ± 0.3	14.3 ± 1.7	9.56	9.57
A963	10:17:14.2, +39:01:24.0	2.53	1392.2 ± 41.8			26.8 ± 2.8	9.32	8.31
A2261	17:22:16.9, +32:09:10.4	2.46	24.3 ± 1.6	10.48 ± 0.16		8.7 ± 1.1	10.79	10.18
	17:22:23.8, +32:01:26.4	6.56	126.7 ± 4.4			9.3 ± 3.4		
MACS J2214.9	22:14:39.3, −14:00:58.5	4.44	58.4 ± 1.8	107.10 ± 0.58		51.4 ± 5.2	12.86	12.60

Notes. Point sources detected in Bolocam cluster observations with S/N > 4 in SZ-model-subtracted beam-smoothed images. The uncertainties given above fully account for degeneracies between the point source and the SZ model, and are therefore larger than the noise RMS in the beam-smoothed images. As a result, our constraint on the flux density of one source has an S/N < 4. Note that, in contrast to the central point sources selected from NVSS, 5/6 of these sources appear to be flat-spectrum sources. This is due to the fact that most steep-spectrum sources are too dim to be detected in our 140 GHz data.

of the BCGs are detected in one or more *Herschel* bands, and graybody fits of the *Herschel* data result in extrapolated flux densities at our observing band of <0.1 mJy for all but two of these sources. Based on our analysis of the contamination from central radio galaxies, even these brightest dusty sources would result in <1% fractional changes in the SZ S/N. In summary, the dust emission sourced by cluster-member galaxies in our images is likely to be negligible, and we therefore do not account for it in this analysis.

5. RADIO SOURCES DIRECTLY DETECTED BY BOLOCAM

The number of cluster-member radio galaxies drops quickly with radius from the cluster center (Coble et al. 2007; Muchovej et al. 2010), and the blank-sky description of the source population becomes approximately correct at these larger radii. Over the full set of 45 clusters we map a fairly significant area ($\simeq$2.5 deg^2), which is enough to contain a handful of very bright radio sources (Vieira et al. 2010; Marriage et al. 2011b). Fortunately, we are able to easily detect and subtract these sources from our data because they have little or no degeneracy with our template of the SZ signal. We search for these sources by selecting pixel excursions with an S/N > 4 in maps that have had the best-fit SZ template subtracted and are beam-smoothed for improved point-source extraction. We find 15 such excursions, 12 with positive flux density and three with negative flux density. Six of these positive flux candidates have counterparts in NVSS, and we estimate the 140 GHz flux density of each of these sources by fitting a point-source template to our maps using the NVSS coordinates as a prior (Condon et al. 1998). The dimmest of the sources with NVSS associations have flux densities of $\lesssim$10 mJy in our images, providing a rough estimate of our detection threshold (see Table 4). Although our detection threshold is not uniform due to residual SZ contamination, the varying depths of our maps, and the tapered coverage within our maps, the SPT source counts measured by Vieira et al. (2010) indicate we should see $\simeq$2 sources above 10 mJy in our maps. Therefore, we detect approximately three times as many bright radio sources as expected, although this excess is not significant due to the small number of sources.

For the five clusters that contain these six radio sources we have computed the SZ S/N both before and after subtraction of the source(s). Note that in all cases we have removed the bright central radio sources described in Table 3. These six radio sources are located at a range of positions relative to the cluster centers (between 2.5 and 6.6 arcmin), and have 140 GHz flux densities between 8.7 and 51.4 mJy. In most cases, the SZ S/N decreases after subtraction of the radio source(s), due to the fact that the radio source(s) are mainly in the ring of positive flux surrounding the SZ decrement caused by the high-pass filtering applied to the data. In the extreme case of A963, with a 26.8 mJy radio source located only 2.5 arcmin from the cluster center, the fractional change in the SZ S/N is 12%. However, the median fractional change in SZ S/N due to these bright sources is $\simeq$2.5%. If we therefore assume that a source brighter than 2.5 times below our detection threshold would be required to produce a >1% fractional change in the SZ S/N, then based on the results of Vieira et al. (2010) we expect 2–3 such sources among our sample of 45 clusters. Therefore, given the results of Section 3.3, where 13 clusters had central radio galaxies that produced a >1% change in the SZ S/N, contamination from undetected back/foreground radio galaxies should be a factor of $\simeq$5 below the contamination from central cluster-member radio galaxies.

After removing the six sources with NVSS associations, we are left with nine unassociated pixels (six positive and three negative). All of these unassociated pixels have S/N just above 4. Statistically, based on Gaussian noise, we only expect $\simeq$1 noise excursion with S/N > 4, and it is unclear why we have nine such excursions. However, we do note that most of our images have significant SZ signal in them (S/N > 10), and relatively modest differences between our SZ model and the underlying cluster profile could therefore combine with noise excursions in some clusters and cause such high S/N pixels in our best-fit-SZ-model-subtracted images. In addition, the noise in our images is not perfectly white, and large-angular-scale noise could also be responsible for some of these S/N > 4 pixels. Given that our data show an excess of bright radio sources exclusive of these nine unassociated pixels, we assume that they are the result of one of the non-idealities mentioned above rather than an actual radio source. We do not attempt to further account for these nine unassociated pixels with S/N > 4.

6. CONCLUSIONS

Using a combination of 140 GHz Bolocam data, 1.4 GHz NVSS data, and $\simeq$30 GHz data from OVRO/BIMA and SZA, we have studied the 140 GHz emission from cluster-member galaxies in a sample of 45 massive clusters. In agreement with previous results, we find that cool-core clusters preferentially host more radio galaxies and that all of the cluster-member galaxies have steep spectra. On average, we find that the spectral index between 30 and 140 GHz is consistent with, but slightly steeper than, the spectral index between 1.4 and 30 GHz. We

further find that galaxy-to-galaxy variations lead to a $\simeq$30% scatter in 140 GHz flux densities extrapolated from data below 30 GHz. Based on an extrapolation to 140 GHz from the lower frequency data, we find that only $\simeq 1/4$ of the clusters contain enough radio emission to produce more than a 1% bias in the optimally filtered peak SZ signal from the cluster, and the maximum contamination in a single cluster is $\simeq$20%. However, we do note that the contamination in cool-core systems is significantly enhanced compared with the sample average. These results roughly match expectations from lower frequency measurements and simulations (Lin et al. 2009; Sehgal et al. 2010; Andersson et al. 2011) and indicate that the amount of radio contamination in high-mass clusters is small compared with achieved noise levels in SZ measurements obtained at 140 GHz.

We acknowledge the assistance of the day crew and Hilo staff of the Caltech Submillimeter Observatory, who provided invaluable assistance during data taking for this data set; Mike Zemcov, Dan Marrone, and John Carlstrom for useful discussions; Max Bonamente, John Carlstrom, Thomas Culverhouse, Christopher Greer, Marshall Joy, James Lamb, Erik Leitch, Dan Marrone, Amber Miller, Thomas Plagge, Matthew Sharp, and David Woody for providing OVRO/BIMA and/or SZA data for our analysis; Kathy Deniston, Barbara Wertz, and Diana Bisel, who provided effective administrative support at Caltech and in Hilo; Matt Hollister and Matt Ferry, who assisted in the collection of these data; and the referee for useful suggestions that significantly improved our manuscript. The Bolocam observations were supported by the Gordon and Betty Moore Foundation. J.S. was supported by a NASA Graduate Student Research Fellowship, a NASA Postdoctoral Program Fellowship, NSF/AST-0838261 and NASA/NNX11AB07G; T.M. was supported by NASA through the Einstein Fellowship Program grant PF0-110077; N.C. was partially supported by a NASA Graduate Student Research Fellowship; A.M. was partially supported by NSF/AST-0838187; S.A., E.P., and J.A.S. were partially supported by NASA/NNX07AH59G; and K.U. acknowledges support from the Academia Sinica Career Development Award. A portion of this research was carried out at the Jet Propulsion Laboratory, California Institute of Technology, under a contract with the National Aeronautics and Space Administration. This research made use of the Caltech Submillimeter Observatory, which is operated by the California Institute of Technology under cooperative agreement with the National Science Foundation (NSF/AST-0838261). The operation of the SZA was supported by NSF/AST-0838187, and CARMA operations were supported by the CARMA partner universities under a cooperative agreement with the National Science Foundation.

REFERENCES

Andersson, K., Benson, B. A., Ade, P. A. R., et al. 2011, ApJ, 738, 48
Arnaud, M., Pratt, G. W., Piffaretti, R., et al. 2010, A&A, 517, A92
Bai, L., Macillac, D., Rieke, G. H., et al. 2007, ApJ, 664, 181
Béthermin, M., Dole, H., Lagache, G., Le Borgne, D., & Penin, A. 2011, A&A, 529, A4
Blain, A. W., Smail, I., Ivison, R. J., Kneib, J.-P., & Frayer, D. T. 2002, PhR, 369, 111
Bock, D. C.-J., Large, M. I., & Sadler, E. M. 1999, AJ, 117, 1578
Böhringer, H., Pratt, G. W., Arnaud, M., et al. 2010, A&A, 514, A32
Bolton, R. C., Chandler, C. J., Cotter, G., et al. 2006, MNRAS, 370, 1556
Bonamente, M., Hasler, N., Bulbul, E., et al. 2012, NJPh, 14, 025010
Coble, K., Bonamente, M., Carlstrom, J. E., et al. 2007, AJ, 134, 897
Cohen, A. S., Lane, W. M., Cotton, W. D., et al. 2007, AJ, 134, 1245
Condon, J. J., Cotton, W. D., Greisen, E. W., et al. 1998, AJ, 115, 1963
Cooray, A. R., Grego, L., Holzapfel, W. L., Joy, M., & Carlstrom, J. E. 1998, AJ, 115, 1388
Das, S., Marriage, T. A., Ade, P. A. R., et al. 2011, ApJ, 729, 62
de Zotti, G., Massardi, M., Negrello, M., & Wall, J. 2010, A&ARv, 18, 1
Finn, R. A., Desai, V., Rudnick, G., et al. 2010, ApJ, 720, 87
Geach, J. E., Smail, I., Ellis, R. S., et al. 2006, ApJ, 649, 661
Glenn, J., Bock, J. J., Chattopadhyay, G., et al. 1998, Proc. SPIE, 3357, 326
Gold, B., Odegard, N., Weiland, J. L., et al. 2011, ApJS, 192, 15
Griffith, M. R., Wright, A. E., Burke, B. F., & Ekers, R. D. 1994, ApJS, 90, 179
Haig, D. J., Ade, P. A. R., Aguirre, J. E., et al. 2004, Proc. SPIE, 5498, 78
Kellermann, K. 1996, ApJ, 146, 621
Komatsu, E., Kitayama, T., Suto, Y., et al. 1999, ApJL, 516, L1
Large, M. I., Mills, B. Y., Little, A. G., Crawford, D. F., & Sutton, J. M. 1981, MNRAS, 194, 693
Lin, Y.-T., Partridge, B., Pober, J. C., et al. 2009, ApJ, 694, 992
Mantz, A. 2009, PhD thesis, Stanford Univ.
Mantz, A., Allen, S. W., Ebeling, H., Rapetti, D., & Drlica-Wagner, A. 2010, MNRAS, 406, 1773
Marcillac, D., Rigby, J. R., Rieke, G. H., & Kelly, D. M. 2007, ApJ, 654, 825
Marriage, T. A., Acquaviva, V., Ade, P. A. R., et al. 2011a, ApJ, 737, 61
Marriage, T. A., Baptiste, J. J., Lin, Y.-T., et al. 2011b, ApJ, 731, 100
Massardi, M., Bonaldi, A., Negrello, M., et al. 2010, MNRAS, 404, 532
Massardi, M., & de Zotti, G. 2004, A&A, 424, 409
Mauch, T., Murphy, T., Buttery, H. J., et al. 2003, MNRAS, 342, 1117
Maughan, B. J., Giles, P. A., Randall, S. W., Jones, C., & Forman, W. R. 2012, MNRAS, 421, 1583
Maughan, B. J., Jones, C., Forman, W., & Van Speybroeck, L. 2008, ApJS, 174, 117
Mittal, R., Hudson, D. S., Reiprich, T. H., & Clarke, T. 2009, A&A, 501, 835
Muchovej, S., Leitch, E., Carlstrom, J. E., et al. 2010, ApJ, 716, 521
Muchovej, S., Mroczkowski, T., Carlstrom, J. E., et al. 2007, ApJ, 663, 708
Murphy, T., Mauch, T., Green, A., et al. 2007, MNRAS, 382, 382
Planck Collaboration 2011a, A&A, 536, A8
Planck Collaboration 2011b, A&A, 536, A13
Pointecouteau, E., Giard, M., Benoit, A., et al. 2001, ApJ, 552, 42
Pratt, G. W., Croston, J. H., Arnaud, M., & Böringer, H. 2009, A&A, 498, 361
Rawle, T. D., Edge, A. C., Egami, E., et al. 2012, ApJ, 747, 29
Reese, E. D., Carlstrom, J. E., Joy, M., et al. 2002, ApJ, 581, 53
Reichardt, C. L., Shaw, L., Zahn, O., et al. 2012a, ApJ, 755, 70
Reichardt, C. L., Stalder, B., Bleem, L. E., et al. 2012b, arXiv:1203.5775
Ricci, R., Prandoni, I., Gruppioni, C., Sault, R. J., & de Zotti, G. 2006, A&A, 445, 465
Sadler, E. M., Ricci, R., Ekers, R. D., et al. 2006, MNRAS, 371, 898
Sadler, E. M., Ricci, R., Ekers, R. D., et al. 2008, MNRAS, 385, 1656
Sajina, A., Partridge, B., Evans, T., et al. 2011, ApJ, 732, 45
Sayers, J., Czakon, N. G., Bridge, C., et al. 2012a, ApJL, 749, L15
Sayers, J., Czakon, N. G., & Golwala, S. R. 2012b, ApJ, 744, 169
Sayers, J., Czakon, N. G., Mantz, A., et al. 2012c, arXiv:1211.1632
Sayers, J., Golwala, S. R., Ameglio, S., & Pierpaoli, E. 2011, ApJ, 728, 39
Sehgal, N., Bode, P., Das, S., et al. 2010, ApJ, 709, 920
Sun, M. 2009, ApJ, 704, 1586
Sunyaev, R. A., & Zel'dovich, Y. B. 1972, CoASP, 4, 173
Tingay, S. J., Jauncey, D. L., King, E. A., et al. 2003, PASJ, 55, 351
Tucci, M., Toffolatti, L., de Zotti, G., & Martínez-González, E. 2011, A&A, 533, A57
Vanderlinde, K., Crawford, T. M., de Haan, T., et al. 2010, ApJ, 722, 1180
Vieira, J. D., Crawford, T. M., Switzer, E. R., et al. 2010, ApJ, 719, 763